# An incompressible Eulerian formulation for soft solids in fluids

**By S. S. Jain AND A. Mani**

## 1. Motivation and objectives

Soft solids in fluids are ubiquitous in nature. Studies of these systems are of practical relevance in science and engineering. Some of the applications of this system involve the study of the interaction between micro-bubble collapse-induced shock waves with the tissue in an animal body, where the tissue can be modeled as a soft solid in blood, the study of the electroporation phenomenon, where the cell membrane can be modeled as a solid surrounded by fluid medium.

A solid-fluid coupled system, also known as a fluid-structure interaction (FSI) problem, has historically been studied using a Lagrangian approach for the solid and an Eulerian approach for the fluid regions (see the, arbitrary Lagrangian-Eulerian approach of Hu *et al.* (2001)), but the method found success mostly in the stiff limit of the solids and was found to be too cumbersome for highly deforming solids. Efforts to couple fluids and solids on a single Eulerian grid have also been attempted, but with limited success. For example, the classical immersed boundary method (Peskin 1982), the cut-cell finite volume approach (Clarke *et al.* 1986) and the immersed interface method (LeVeque & Li 1994) all use a single Eulerian grid, but in most of these methods a deforming solid is considered as a boundary condition to solve for the fluid region, or a simple Hooke's law (a spring model) is used to approximate the deformation of the the solids.

Fully Eulerian approaches that can solve solids using true solid constitutive laws in solid regions coupled with fluid flow have been developed before but were limited to unbounded domains (see the, Eulerian Godunov method of Miller & Colella (2001)). A recent work by Kamrin *et al.* (2012) introduced the reference map technique (RMT), a fully Eulerian approach to the simulation of solids and an extension to FSI problems (Valkov *et al.* 2015). These authors simulated soft solids on a staggered grid in a compressible flow setting. We adopt the incompressible version of this formulation and assess various improvements to the original RMT method.

Here, we present an accurate reference map technique (Jain & Mani 2017) for the simulation of incompressible soft solids in fluids. We discuss the improvements made in terms of the accuracy, cost, easy of implementation and robustness of the method and also discuss some of the best modeling practices. In what follows, we describe this improved formulation, adopting a heuristic approach.

## 2. Eulerian formulation for solids and fluids

### 2.1. *Reference map technique*

Consider a solid in convective coordinate system, as shown in Figure 1. At time $t = 0$, the solid is in its initial configuration (reference configuration), represented by $\Omega_0$, and at time $t > 0$, the solid is in its deformed configuration, represented by $\Omega_t$ after being displaced and deformed by external forces. If, $\vec{X}$ represents a position vector in $\Omega_0$ that points to

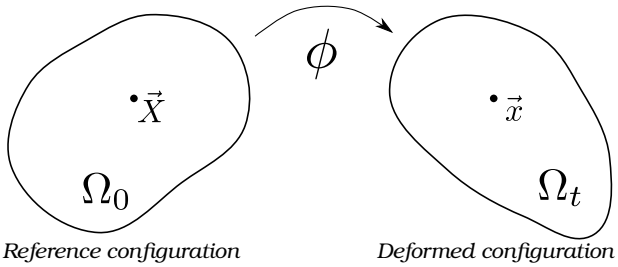


FIGURE 1. Schematic of a deforming solid in a convective coordinate system.

a material particle, then this material particle in $\Omega_t$ has the same $\vec{X}$ associated with it, since $\vec{X}$ represents the initial coordinates of the point in $\Omega_0$. Let $\vec{x}$ be the corresponding position vector in $\Omega_t$. Then, defining a vector field (a reference map) $\vec{\xi}(\vec{x},t)$ as

$$\vec{\xi}(\vec{x},t) = \vec{X}, \tag{2.1}$$

The material derivative of this yields

$$\frac{D\vec{\xi}(\vec{x},t)}{Dt} = 0. \tag{2.2}$$

Expressing this in terms of the local derivatives, we obtain an advection equation for the $\vec{\xi}(\vec{x},t)$ field as

$$\frac{\partial\vec{\xi}(\vec{x},t)}{\partial t} + \vec{u}.\vec{\nabla}\vec{\xi}(\vec{x},t) = 0. \tag{2.3}$$

This equation can be integrated in time given the initial condition $\vec{\xi}(\vec{x},t=0) = \vec{x} = \vec{X}$. Thus, $\vec{\xi}(\vec{x},t)$ acts as a tag for all the points in the solid, and the kinematic condition in Eq. (2.3) can be used to track every point in the solid, given its initial coordinates. Stress and strain in solid constitutive laws are typically expressed in terms of the material deformation gradient $\mathbb{F}$. Hence, relating $\mathbb{F}$ to $\vec{\xi}(\vec{x},t)$ as

$$\mathbb{F}(\vec{X},t) = \partial\vec{x}/\partial\vec{X} = (\overrightarrow{\nabla}\overrightarrow{\xi}[\vec{x},t)]^{-1} \tag{2.4}$$

lets one express the stress and strain tensors in terms of this new primitive variable $\vec{\xi}(\vec{x},t)$. Eqs. (2.1)-(2.4) in combination give rise to a novel idea to track all the material points in a solid and close the system of equations to model a solid on an Eulerian grid.

### 2.2. *Governing equations for solids and fluids*

In an Eulerian formulation, momentum balance equation for both fluids and solids can be written as

$$\frac{\partial(\rho\vec{u})}{\partial t} + \vec{\nabla}.(\rho\vec{u}\otimes\vec{u}) = \vec{\nabla}.\underline{\underline{\sigma}}, \tag{2.5}$$

where $\vec{u}$ is the global velocity field and the mass balance for fluids (continuity equation) is

$$\frac{\partial\rho}{\partial t} + \vec{\nabla}.(\vec{u}\rho) = 0, \tag{2.6}$$

which in the incompressible limit reduces to $\vec{\nabla}.\vec{u} = 0$. Similarly, the mass balance for solids can be written as $\rho = \rho_o[det(\mathbb{F})]^{-1}$, and in the incompressible limit it reduces to $det(\mathbb{F}) = 1$, implying that the $\rho = \rho_0$. Here, $\underline{\underline{\sigma}}$ is the Cauchy stress and $\rho$ and $\rho_o$ are the density of the deformed and reference configurations, respectively.

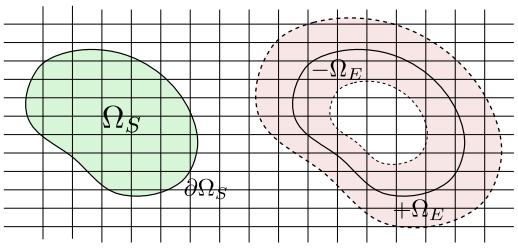


FIGURE 2. Schematic of a solid on an Eulerian grid. $\Omega_E \approx 6\Delta x$,$\Omega_T \approx 3\Delta x$.

For solids, the Cauchy stress can be expressed as a function of strain given by

$$\underline{\underline{\sigma}} = (det\mathbb{F})^{-1}\mathbb{F}\frac{\partial\bar{\psi}(\mathbb{E})}{\partial\mathbb{E}}\mathbb{F}^T = 2(det\mathbb{F})^{-1}\mathbb{F}\frac{\partial\hat{\psi}(\mathbb{C})}{\partial\mathbb{C}}\mathbb{F}^T, \tag{2.7}$$

where $\mathbb{E} = (1/2)(\mathbb{F}^T\mathbb{F} - \mathbb{1})$ is the Green's finite strain tensor, $\mathbb{C} = \mathbb{F}^T\mathbb{F}$ is the right Cauchy-Green's deformation tensor and $\psi(\mathbb{F}) = \hat{\psi}(\mathbb{E}) = \bar{\psi}(\mathbb{C})$ is the Strain energy density function. We use the incompressible neo-Hookean constitutive model for a solid given by

$$\hat{\psi}(\mathbb{C}) = \mu^s(tr\mathbb{C} - 3), \tag{2.8}$$

where $\mu^s = E/2(1+\nu)$ is the shear modulus, $E$ is Young's modulus and $\nu$ is the Poisson ratio. With this, the $\underline{\underline{\sigma}}$ reduces to a simple form given by $\underline{\underline{\sigma}} = 2\mu^s\mathbb{b}$, where $\mathbb{b}$ is the left Cauchy-Green's deformation tensor. Further more, it can be shown that

$$\underline{\underline{\sigma}} = 2\mu^s[(\vec{\nabla}\vec{\xi})^T(\vec{\nabla}\vec{\xi})]^{-1}. \tag{2.9}$$

For fluids, the Cauchy stress can be expressed as a function of the rate of strain. We use the Newtonian constitutive model given by

$$\underline{\underline{\sigma}} = \mu^f\left[\left(\vec{\nabla}\vec{u}\right) + \left(\vec{\nabla}\vec{u}\right)^T\right] - \mathbb{1}P, \tag{2.10}$$

where $P$ is the pressure. To close the system of equations for fluid-solid coupled simulations, we solve a conservative variable-density formulation of the above system of equations along with a mixture model (see, Section 3.3).

## 3. Numerical method and implementation

### 3.1. *Basic methodology*

Consider a solid on an Eulerian grid, as shown in Figure 2. Here, $\Omega_S$ represents the region inside the solid, $\partial\Omega_S$ represents the boundary of the solid, $\pm\Omega_E \approx 6\Delta x$ represents a narrow band region around $\partial\Omega_S$, an extended solid region, and $\pm\Omega_T \approx 3\Delta x$ represents another narrow band region around $\partial\Omega_S$, a transition zone (not shown in the Figure 2). Since, both solid and fluid regions are solved together in a coupled fashion, they share the same grid and a global velocity field. In the regions of solid $\Omega_S$, stress is computed using the solid constitutive law, and outside this region, stress is computed using the fluid constitutive law. Once the stress for solid and fluid regions is evaluated, global stress is computed by appropriately blending the solid and fluid stresses in a narrow band region ($\Omega_T$) around the solid boundary, and finally the velocity field is updated by solving the discretized version of Eq. (2.5) and by projecting the velocity field onto a divergence-free field.

An important thing to note is that $\vec{\xi}$ is the variable that contains the history of the material and its origin. This field quickly becomes invalid in the regions of fluid due to the highly nonlinear deformation behavior of the fluids. Hence, $\vec{\xi}$ is defined only within the solid region, and to evaluate the solid stress in $\Omega_T$, the $\vec{\xi}$ field is appropriately extrapolated into the regions outside the solid (into $\Omega_E$).

Valkov *et al.* (2015), used the hyperbolic PDE approach of Aslam (2004) to extrapolate the $\vec{\xi}$ field. Hereafter, we refer to this approach as RMT. This approach assumed that a level-set field is known in the region of extrapolation. By contrast, we use a least-squares-based extrapolation procedure (explained later) that does not require a known level-set field in the region of extrapolation. However, a local level-set field $\phi$ has to be defined in the $\Omega_E$ region, which is used in defining the Heaviside function required for the mixture model and also in enforcing the solid-solid and solid-wall contact boundaries.

#### 3.1.1. *Projection method loop*

We use a finite-volume approach on a fully collocated Cartesian grid to discretize our system of equations. Hence, all our primary variables ($\vec{\xi}$,$\vec{u}$,$P$) are stored on the cell center. We modify the approximate projection method of Almgren *et al.* (2000) to incorporate the coupled solution of solid and fluid regions. The steps involved in our projection method loop are as shown in Algorithm 1.

A second-order central differencing scheme (CDS), or Superbee scheme, is used to compute the fluxes in the advection equations for both $\vec{\xi}$ and $\vec{u}$, and they are solved using an RK-4 time integration scheme. The diffusion equation for $\vec{u}$ is split from the advection part, as shown in Eq. (5.2) and a forward-Euler time integration is used to solve this step. We use the second-order central difference approximation to evaluate the gradient tensor ($\vec{\nabla}\vec{\xi}$) in Eq. (2.9). For example, in a two-dimensional Cartesian case

$$(\vec{\nabla}\vec{\xi})_{11} = \frac{\xi_{x(i+1,j)} - \xi_{x(i-1,j)}}{2}, \tag{3.1}$$

where $\xi_x = \vec{\xi}.\hat{i}$. Note that RMT used one-sided differences to evaluate the gradient tensor. The divergence of Cauchy stress in Eq. (5.2) is also computed using CDS.

### 3.2. *Reference map and level-set field*

#### 3.2.1. *Level-set reconstruction*

As explained in the previous section, a level-set field $\phi$ is required to be defined at every time step in the $\Omega_E$ region. One way to define $\phi(\vec{x},t)$ is to advect $\phi$ using the standard level-set advection equations given $\phi(\vec{X}, t = 0)$. This approach was adopted by RMT, leading to a mismatch between the $\phi(\vec{x},t) = 0$ and the boundary of the solid defined by $\vec{\xi}(\vec{x},t)$ field, which resulted in a wrinkled solid-fluid interface and hence affected the quality of extrapolation. The authors solved this issue by defining additional routines to smooth out the striations in the extrapolated regions. This approach could also potentially lead to mass conservation issues. By contrast, a simpler, exact, conservative and also cost-effective way to define $\phi(\vec{x},t)$ is to reconstruct it from the known field at $t = 0$, utilizing the known $\vec{\xi}(\vec{x},t)$ field at time $t$ using a simple condition given by

$$\phi(\vec{x},t) = \phi[\vec{\xi}(\vec{x},t), t = 0]. \tag{3.2}$$

Since an analytical expression can be defined for $\phi(\vec{X}, t = 0)$ for simple-shaped solids, the above equation yields an exact field for $\phi(\vec{x},t)$ for a given $\vec{\xi}(\vec{x},t)$, thus maintaining

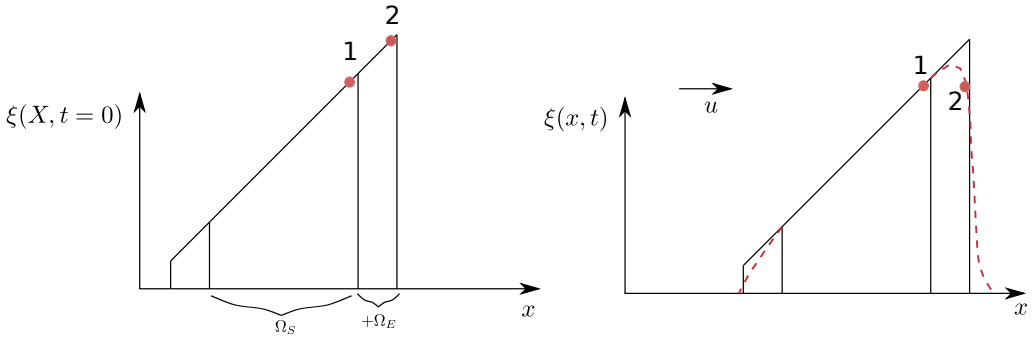


FIGURE 3. Schematic of a one-dimensional solid solved without the modified advection equation.

a perfect match between the $\phi(\vec{x}, t) = 0$ surface and the boundary of the solid defined by $\vec{\xi}(\vec{x}, t)$, which is crucial in developing a robust solver. If an analytical expression for $\phi(\vec{X}, t = 0)$ is not available, then a bilinear interpolation (in two-dimensions) can be used to calculate $\phi(\vec{\xi}(\vec{x}, t), t = 0)$.

3.2.2. *Modified reference map advection*

The reference map field $\vec{\xi}$ is advected using Eq. (2.3). As explained in the previous section, $\vec{\xi}$ is defined and advected only within the $\Omega_S$. This can be conveniently achieved by modifying Eq. (2.3) into

$$\frac{\partial \vec{\xi}(\vec{x}, t)}{\partial t} + H(\vec{x})\vec{u}.\vec{\nabla}\vec{\xi}(\vec{x}, t) = 0, \tag{3.3}$$

where $H(\vec{x})$ is a Heaviside function defined as

$$H(\vec{x}) = \begin{cases} 1 & \Omega_S \\ 0 & \text{else.} \end{cases} \tag{3.4}$$

This modification to the advection equation of $\vec{\xi}$ has multiple advantages; the very obvious one is that this approach effectively eliminates the high-frequency content in the $\vec{\xi}$ field, resulting in an ability to use simple schemes such as CDS to compute the fluxes, without losing the accuracy of the solution. To realize the second advantage, which is not very obvious, consider the $\vec{\xi}$ field of a one-dimensional solid, as shown in Figure 3.

At time $t = 0$, $\vec{\xi}$ is a simple straight line ($\xi = x$) and is given as an input to the solver, as shown on the left. Let $u$ denote the velocity field; then after time $t$, an ideal solid would have advected to a new location, shown on the right, maintaining the shape (solid line). If the modified equation shown in Eq. (3.3) is not used to advect, then a Total Variation Diminishing (TVD) type scheme can be used to compute the fluxes, which artificially add diffusivity to the equation to stabilize the solver. This results in the profile shown on the right with dotted lines. If this profile is obtained as a result of advection, then the reconstruction step of the level-set field using Eq. (3.2) breaks down. To understand this, consider the two solid circles 1 and 2 in the Figure 3. Circle 1 is inside the solid in $\Omega_S$ at $t = 0$, but circle 2 is outside the solid in $\Omega_E$. After advection, circle 1 still represents a value of $\xi$ inside the solid, whereas circle 2 represents a value of $\xi$ that was originated due to numerical diffusion and denotes that it is inside solid

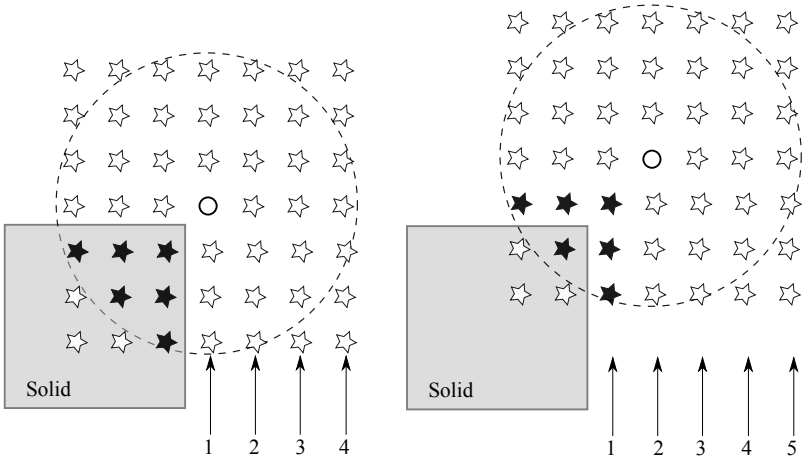


FIGURE 4. Schematic of the traversal procedure for least-squares extrapolation. Numbers represent the passes. The left-hand side shows the state of the system before the first pass, and the right-hand side is the state after the first pass. The stars represent cell center locations, filled stars represent the cells where the values are already known and the solid circle represents the cell where the extrapolation is needed.

region $\Omega_S$. Hence, to clip the values of $\xi$ outside the solid region before extrapolation $\xi$, the boundaries of the solid needs to be identified. This can be done using the level-set field constructed using Eq. (3.2) (which takes $\xi$ as the input). This procedure (without the modified advection equation) typically creates two boundaries for the solid, leading to the failure of the method. Thus using the modified advection equation for $\vec{\xi}$ effectively eliminates this issue by clipping the values of $\vec{\xi}$ outside the solid right in the advection step. As a result, $\vec{\xi}$ can be extrapolated without any need for clipping.

3.2.3. *Least-squares-based extrapolation*

RMT used a hyperbolic PDE approach to extrapolate the $\vec{\xi}$ field outside the solid regions into $\Omega_E$. We derive a simpler, more cost-effective approach to extrapolate the $\vec{\xi}$ field. It is based on the assumption that the $\vec{\xi}$ field is locally linear, even in the deformed state of the solid. Consider the solid represented by a square (in two-dimensions) in Figure 4. Consider the dashed circle of radius $4r$ as the stencil, where $r = \sqrt{\Delta x^2 + \Delta y^2}$. Hence a plane of the form $\xi = ax + by + c$ can be fit for the known cell values, where $x$, $y$ and $\xi$ represent the coordinate location and the reference map value of the cells and $a$, $b$ and $c$ are the coefficients to be determined, thus forming an over-determined system that can be solved using the least-squares approach. The stencil's radius was chosen to make the system over-determined for all the possible configurations. Once the coefficients are calculated, the value of $\xi$ at the solid circle can be computed. The procedure begins by repeatedly solving least-squares systems for all the cells adjacent to the cells for which the value of $\xi$ is already known. This is considered the first pass. This pass is repeated until the required width of the extrapolated region is obtained. This cell traversal procedure is summarized in Algorithm 2.

### 3.3. *Closure model*

The level-set field $\phi$ reconstructed using Eq. (3.2) should be reinitialized to restore its signed-distance property. We solve the Eikonal equation by adopting the fast marching method of Chopp (2001) to reinitialize the $\phi$ field. The coupled fluid-solid system of

| | RMT (Valkov *et al.* 2015) | Present approach |
|---|---|---|
| Grid | Staggered | Collocated |
| Nature of the solver | Compressible | Incompressible |
| Reference map extrapolation | PDE based | Least-squares based |
| Level-set construction | Advected in time | Reconstructed from $t = 0$ (Analytical—exact) |
| Level-set reinitialization | PDE based | Fast Marching Method |
| Smoothing routines | Required | No |
| Discretization stencil | One-sided | Central |
| Global damping | Yes | No |

TABLE 1. Comparison between the present method and RMT.

equations is closed by defining the mixture model inspired by the one-fluid formulation as

$$\underline{\underline{\sigma}} = H[\phi(\vec{x},t)]\underline{\underline{\sigma}}^f + \{1 - H[\phi(\vec{x},t)]\}\,\underline{\underline{\sigma}}^s,$$

$$\rho = H[\phi(\vec{x},t)]\rho^f + \{1 - H(\phi(\vec{x},t))\}\,\rho^s,$$

where $\phi$ is the reinitialized level-set field and $H(x)$ represents a Heaviside function defined as

$$H(x) = \begin{cases} 0 & x \le -w_T \\ \dfrac{1}{2}\left[1 + \dfrac{x}{w_T} + \dfrac{1}{\pi} sin(\dfrac{\pi x}{w_T})\right] & |x| < w_T \\ 1 & x \ge w_T, \end{cases} \tag{3.5}$$

where $w_T$ represents the width of the transition region $\Omega_T$. For $n$ number of solids, this model can be extended accordingly

$$\underline{\underline{\sigma}} = \Big\{ \sum_{i=1}^{n} H_i[\phi(\vec{x},t)] - n + 1 \Big\}\underline{\underline{\sigma}}^f + \sum_{i=1}^{n} \Big\{1 - H_i[\phi(\vec{x},t)]\Big\}\underline{\underline{\sigma}}^s. \tag{3.6}$$

When two solids collide in a fluid, a fictitious body force needs to be added to the momentum equation to keep them separated and to avoid the inter-penetration of solids. We use the same procedure as RMT to simulate solid-solid contact and solid-wall contact conditions.

Our solver is written in C++ in an object-oriented programming style, and the data files are stored in the legacy Visual ToolKit format (VTK) for visualization purposes. The pressure Poisson system in Eq. (5.4) is solved using the conjugate-gradient solver. Major differences and improvements between our work and that of the RMT are listed in Table 1. Noticeably, we have extended the original reference map technique (RMT) to solve for coupled fluid-solid flow problems on an Eulerian collocated grid and modified the procedure to extrapolate the reference map and level-set reconstruction to improve the cost, accuracy and robustness of the solver.

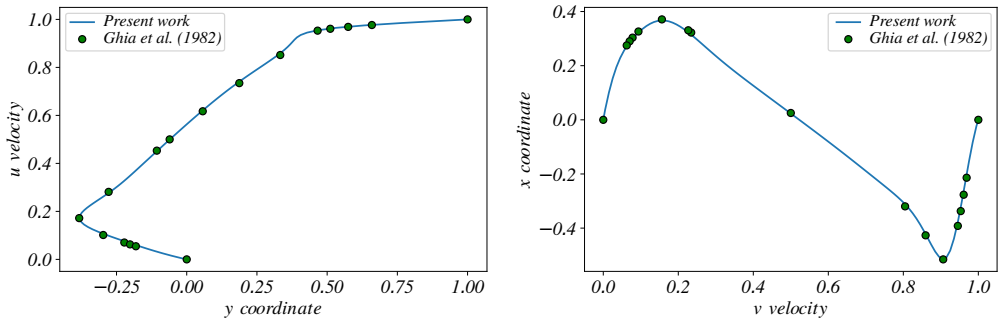


FIGURE 5. Lid-driven test case at $Re = 1000$. (a) The x component of velocity along a vertical line through the center of the domain. (b) The y component of velocity along a horizontal line through the center of the domain.

## 4. Results and discussion

In this section, we present some basic qualitative test cases and a more quantitative study is dedicated for future study. Since the FSI problem involves multiphysics, and an explicit time integration is adopted for solving the system of equations, care must be taken to resolve all the time steps involved in the problem. Time step restriction due to CFL criterion from the advection can be written (for forward Euler in one dimension) as $\Delta t \leq C\Delta x/u$, where $C$ represents the Courant number. Time step restriction from the diffusion equation for fluids yields $\Delta t \leq 0.5\rho^f(\Delta x)^2/\mu^f$. Similarly, the shear wave traveling in the solids needs to be resolved, and the speed of this shear wave is given by, $u = \sqrt{\mu^s/\rho^s}$. Analogously, a time constraint can be defined for solids using this speed as $\Delta t \leq P\Delta x\sqrt{\rho^s/\mu^s}$, where $P$ represents an appropriate pre-factor that depends on the numerical method. The time constraint for the solids turn out to be the most restrictive condition of all, if the ratio of $\mu^s/\rho^s$ is very high. Hence, in the stiff solid limit such as in metals, imposed time step constraints are so strict that the simulation time close to solid length scales is virtually impossible with the explicit time stepping approach. Therefore, this formulation is best suited for the simulation of soft solids in fluids.

### 4.1. *Validation*

The incompressible Navier-Stokes solver on a collocated grid was validated for the lid-driven cavity case against the benchmark results from Ghia *et al.* (1982). A $100 \times 100$ grid was used for the simulation, and the results were reported for Re = 1000. Figure 5 shows a good match of the $u$ and $v$ velocities along the vertical and horizontal lines through the center of the domain with the results from Ghia *et al.* (1982).

Since the equations are solved on a collocated grid, to eliminate the checkerboard fields a Rhie-Chow-like interpolation was performed, as described in Step 5 of the projection method loop (Algorithm 1). Figure 6 presents pseudocolor plots of the velocity and pressure fields from the lid-driven cavity case, illustrating the smoothness of the solution fields obtained.

We compared the accuracy of our least-squares extrapolation procedure with that of the hyperbolic PDE approach used in RMT. Figure 7 shows the schematic of the Zalesak disk test case, wherein a slotted disk (a $\vec{\xi}$ field) is advected with a given background velocity field. The error in the extrapolation procedure manifests as the error in the advection of the $\vec{\xi}$ field. So we computed the $L_2$ norm error $E_\xi = ||\xi_i - \xi_f||_2$ for the

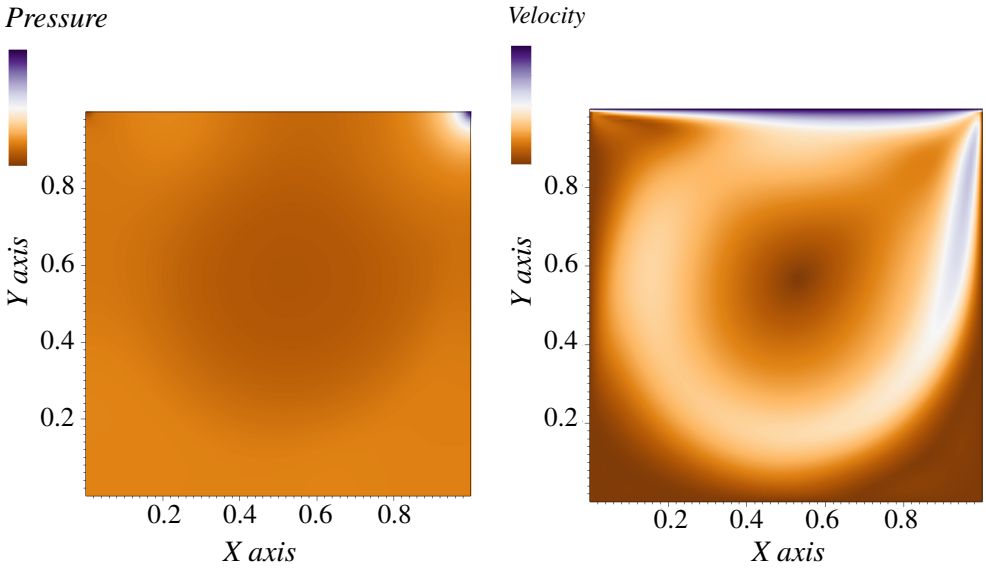


FIGURE 6. Velocity and pressure at $t = 100$ showing no checkerboard oscillations.

| | Least-squares approach | PDE approach |
|---|---|---|
| $E_{\vec{\xi}.\hat{i}}$ | $6.72 \times 10^{-9}$ | $8.32 \times 10^{-4}$ |
| $E_{\vec{\xi}.\hat{j}}$ | $7.34 \times 10^{-9}$ | $4.67 \times 10^{-4}$ |

TABLE 2. Error in the extrapolation procedure.

advection, where $\xi_i$ and $\xi_f$ are the initial and final fields obtained after one full rotation, and report them in Table 2. It is evident that our least-squares procedure is considerably more accurate when compared to the PDE approach.

The above test case was performed on a $100 \times 100$ grid. Moreover, we also compared the cost of the extrapolation procedure using both approaches and found that on average the least-squares procedure took $\approx$ 100ms per extrapolation, whereas the PDE approach took $\approx$ 1550ms per extrapolation on this grid (close to Poisson solve), for an extrapolation band region of $5\Delta x$. This also proves that our least-squares procedure is extremely cost-effective when compared to the PDE approach.

### 4.2. *Simulations of solids in a fluid*

In the rest of the report, we present the simulations of an incompressible solid(s) immersed in a fluid medium. Figure 8 shows a configuration of two separated solids of $\mu^s = 100$ with an initially imposed Taylor-Green vortex field. Two solids collide and separate from each other as expected. A time evolution of the shapes of the two solids colliding is shown in Figure 9. This test case shows the ability of the solver to handle the solid-solid contact situations successfully.

To further demonstrate the robustness of our solver, consider a time instance after collision, as shown in Figure 8. Shading represents the normal stress in the solid. A

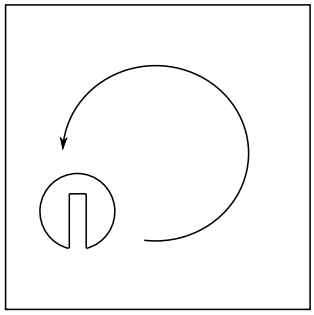

FIGURE 7. Schematic of the rotation of the Zalesak disk test case.

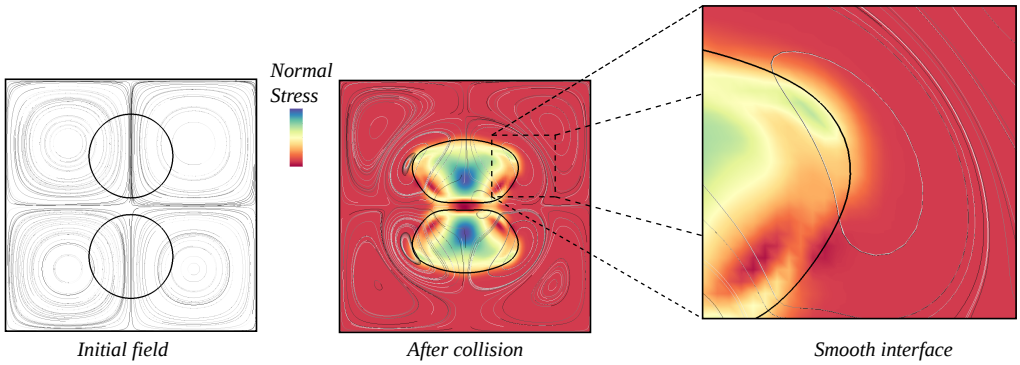


FIGURE 8. Collision of two solids placed in a Taylor-Green vortex, showing the smoothness of the interface and the absence of any striations. Color represents the normal stress $= (\underline{\underline{\sigma}}_{11} + \underline{\underline{\sigma}}_{22})/2$ in the solid.

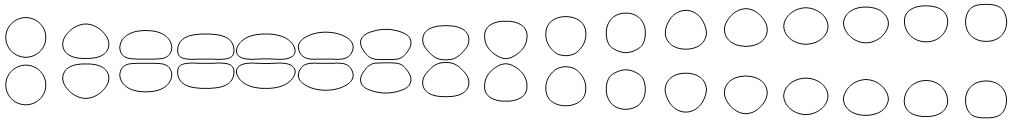

FIGURE 9. Collision of two solids placed in a Taylor-Green vortex.

zoomed-in view of the interface is also shown in the inset. Clearly, the interface between the solid and the fluid here is very smooth (due to an exact match between the level-set field and $\vec{\xi}$ fields at all times; see Section 3.2.1). We also do not see any striations in the extrapolated $\vec{\xi}$ fields that were observed in RMT (see Figure 10 in Valkov *et al.* (2015)), thus eliminating the requirement of the artificial smoothening routine that was used in RMT to remove the striations in the extrapolated region.

To further test the ability of the solver to handle solid-wall contact situations, we performed simulations of the collision of a solid immersed in a fluid with a rigid wall in microgravity and in gravity conditions. Figure 10 shows a soft solid ($\mu^s = 100$) with an initial velocity colliding with a rigid wall and eventually coming to rest due to viscous dissipation in the fluid. Figures 11 and 12 show a stiffer solid ($\mu^s = 1000$) and a soft solid ($\mu^s = 100$) immersed in a fluid and colliding and bouncing off a rigid wall under gravity conditions. Clearly, the softer solid has a lower coefficient of restitution as expected. We leave further quantitative analysis of the results to a future study.

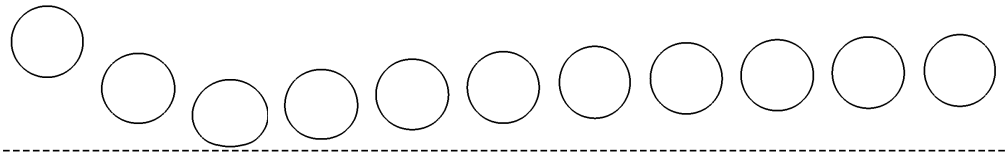

FIGURE 10. Collision of a solid immersed in a fluid with the wall (rigid) in microgravity.

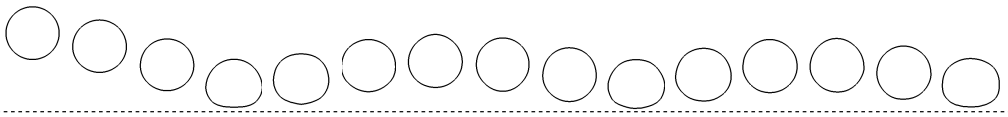

FIGURE 11. Collision of a stiffer solid ($\mu^s = 1000$) immersed in a fluid with the wall (rigid) under gravity.

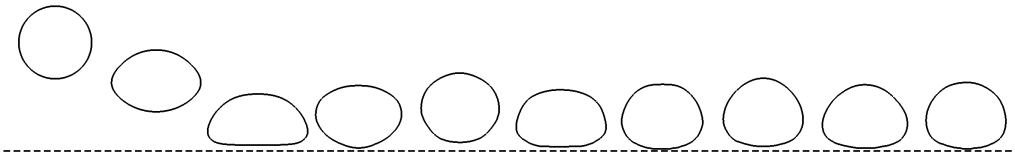

FIGURE 12. Collision of a soft solid ($\mu^s = 100$) immersed in a fluid with the wall (rigid) under gravity.

On a final note, the method used in blending of fluid and solid Cauchy stresses is crucial in obtaining a discretely conservative momentum formulation. For example, one approach is to compute fluid and solid Cauchy stresses, combine them to obtain a global Cauchy stress, and then calculate the divergence of this stress to obtain the force per unit volume due to stresses. The second approach is to compute the divergence of the solid and fluid Cauchy stresses and combine them to obtain the force per unit volume. Obviously the first approach is the one that leads to a conservative formulation, due to the presence of divergence outside the blending operation. This divergence operator, when summed up over adjacent control volumes, leads to an exact cancellation of the terms (analogous to a telescoping series). Hence, we use the conservative formulation in our solver.

A simulation of a solid placed in a Taylor-Green vortex was performed to qualitatively study the differences between these two formulations. Consider Figure 13, which shows the initial state of a solid placed in a Taylor-Green vortex field. As a first guess, we would expect the flow to stretch the solid to some extent, beyond which the stresses developed in the solid retract it and an oscillation mode should set up. We first used the non-conservative formulation, which gave us completely wrong results wherein the solid extends indefinitely, as shown in Figure 14. By contrast, a conservative formulation for the exact same problem yielded correct results, as shown in Figure 15, where the solid oscillates back and forth and goes back to a state of rest after all the energy is lost in viscous dissipation in the fluid.

## 5. Conclusion and future Work

We have presented a conservative, cost-effective and accurate method to simulate soft solids in fluids. The solver is also robust in handling solid-wall and solid-solid contact situations. We have adopted an incompressible version of the reference map technique of

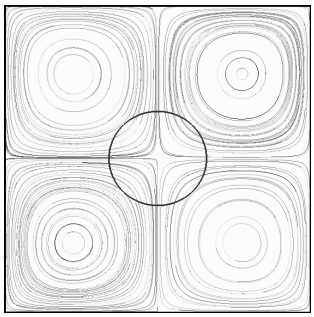

FIGURE 13. Initial state of a solid placed in a Taylor-Green vortex.

FIGURE 14. Extension of a solid placed in an initially Taylor-Green vortex (non-conservative formulation).

FIGURE 15. Oscillation of a solid placed in an initially Taylor-Green vortex (conservative formulation).

Valkov *et al.* (2015) and coupled it with an approximate Projection method (Almgren *et al.* 2000) for the simulation of soft solids in fluids. Furthermore, we have improved the accuracy, cost-effectiveness and robustness of the solver and the ease of implementation by introducing a least-squares extrapolation procedure, a modified advection equation for the reference map field and a simple way to reconstruct the level-set field and by using simple CDS to compute the fluxes. We have presented a state-of-the-art method for the simulation of soft solids in fluids on a collocated Eulerian grid.

This work is not complete; a number of improvements can still be made, such as development of a fully implicit formulation that resolves the difficulty in solving the stiff system, a better kinematic solid-solid contact condition and coupling of the solver with a geometric multigrid algorithm for the Poisson solution.

## Acknowledgments

The first author was supported by a Franklin P. and Caroline M. Johnson Fellowship. The authors are grateful to Prof. Ken Kamrin, MIT for discussions that helped to improve this work.

## Appendix A

**Algorithm 1** Projection method loop

1: Advect reference map and extrapolate using least-squares method.
2: Reconstruct level-set field and reinitialize using Fast-marching method.
3: Compute solid stress and update $\rho$ and $\underline{\underline{\sigma}}$.

4: Solve advection and diffusion to obtain intermediate velocity $\vec{u}_P^{**}$

$$\frac{\rho^{n+1}\vec{u}_P^{*} - \rho^{n}\vec{u}_P^{n}}{\Delta t} = -\vec{\nabla}.\left(\rho\vec{u}_P\vec{u}_P\right)^{n}, \tag{5.1}$$

$$\frac{\rho^{n+1}\vec{u}_P^{**} - \rho^{n+1}\vec{u}_P^{*}}{\Delta t} = \vec{\nabla}.\underline{\underline{\sigma}}(\mu^s, \mu^f, \vec{u}_P^{*}, \vec{\xi}). \tag{5.2}$$

5: Interpolate to obtain face values (Rhie-Chow-like interpolation)

$$\vec{u}_f^{**} = \langle \vec{u}_P^{**} \rangle_{P\to f} - \left\{ \frac{\Delta t}{\rho_f^{n+1}} \left[ \left(\vec{\nabla}P\right)_f^{n} - F_f^{n+1} \right] \right\}, \tag{5.3}$$

where $\langle\rangle_{P\to f}$ is an interpolation from the cell center to the cell face and $F$ is the body force the balanced-force approach of Francois *et al.* (2006)).

6: Solve pressure Poisson equation

$$\vec{\nabla}.\left[ \frac{\left(\vec{\nabla}\delta P\right)_f^{n+1}}{\rho_f^{n+1}} \right] = -\vec{\nabla}.\left( \frac{\vec{u}_f^{**}}{\Delta t} \right), \tag{5.4}$$

where $\delta P$ is the correction for pressure.

7: Update the pressure

$$P^{n+1} = P^{n} + \delta P^{n+1}. \tag{5.5}$$

8: Update the face velocity field —exactly divergence free (to be used in calculating convective fluxes in the next time step)

$$\vec{u}_f^{n+1} = \vec{u}_f^{**} - \left[ \frac{\Delta t}{\rho_f^{n+1}} \left(\vec{\nabla}\delta P\right)_f^{n+1} \right]. \tag{5.6}$$

9: Update the cell center velocity field —approximately divergence free

$$\vec{u}_P^{n+1} = \vec{u}_P^{**} - \Delta t \left\langle \frac{(\vec{\nabla}P)_f - F_f}{\rho_f} \right\rangle_{f\to P}^{n+1}, \tag{5.7}$$

where $\langle\rangle_{f\to P}$ is an interpolation from the cell face to the cell center.

**Algorithm 2** Traversal algorithm

1: Set flag1

$$flag1 = \begin{cases} 1 & \Omega_S \\ 0 & else \end{cases}$$

2: Set flag2

$$flag2 = \begin{cases} 1 & \Omega_S + \Omega_E \\ 0 & else \end{cases}$$

3: Let temp_flag = flag1
4: **for** all cells **do**
5: **if** adjacent neighbour or corner neighbour has flag1 = 1 **then**
6: Solve least-squares system.
7: Update temp_flag.
8: Set flag1 = temp_flag.
9: Repeat 5 to 9 until temp_flag → flag2.

## REFERENCES

Almgren, A. S., Bell, J. B. & Crutchfield, W. Y. 2000 Approximate projection methods: Part I. Inviscid analysis. *SIAM J. Sci. Comput.* **22**, 1139–1159.

Aslam, T. D. 2004 A partial differential equation approach to multidimensional extrapolation. *J. Comput. Phys.* **193**, 349–355.

Chopp, D. L. 2001 Some improvements of the fast marching method. *SIAM J. Sci. Comput.* **23**, 230–244.

Clarke, D. K., Hassan, H. A. & Salas, M. D. 1986 Euler calculations for multielement airfoils using Cartesian grids. *AIAA J.* **24**, 353–358.

Francois, M. M., Cummins, S. J., Dendy, E. D., Kothe, D. B., Sicilian, J. M. & Williams, M. W. 2006 A balanced-force algorithm for continuous and sharp interfacial surface tension models within a volume tracking framework. *J. Comput. Phys.* 213, 141–173.

Ghia, U., Ghia, K. N. & C.T.Shin 1982 High-Re solutions for incompressible flow using the Navier-Stokes equations and a multigrid method. *J. Comput. Phys.* **48**, 387–411.

Hu, H. H., Patankar, N. & Zhu, M. 2001 Direct numerical simulations of fluid—solid systems using the arbitrary Lagrangian —Eulerian technique. *J. Comput. Phys.* **169**, 427–462.

Jain, S. S. & Mani, A. 2017 An update on the Eulerian formulation for the simulation of soft solids in fluids. *Bull. of the Am. Physical Soc.* **62**, BAPS.2017.DFD.L2.7.

Kamrin, K., Rycroft, C. H. & Nave, J. C. 2012 Reference map technique for finite —strain elasticity and fluid-solid interaction. *J. Mech. Phys. Solids* **60**, 1952–1969.

LeVeque, R. J. & Li, Z. 1994 The immersed interface method for elliptic equations with discontinuous coefficients and singular sources. *SIAM J. Numer. Anal.* **31**, 1019–1044.

Miller, G. H. & Colella, P. 2001 A high-order Eulerian Godunov method for elastic-plastic flow in solids. *J. Comput. Phys.* **167**, 131–176.

Peskin, C. S. 1982 The fluid dynamics of heart valves: Experimental, theoretical, and computational methods. *Annu. Rev. Fluid Mech.* **14**, 235–259.

Valkov, B., Rycroft, C. H. & Kamrin, K. 2015 Eulerian Method for multiphase interactions of soft solid bodies in fluids. *J. Appl. Mech.* **82**, 041011.